SOA yields from C$_{10}$ alkanes and oxygenates and their relation to highly oxygenated organic molecules (HOM)

Frans Graeffe[1], Kalle Kupi[1], Hilkka Timonen[2] and Mikael Ehn[1]

[1]Institute for Atmospheric and Earth System Research/Physics, Faculty of Science, University of Helsinki, Helsinki, 00014, Finland

[2]Atmospheric Composition Research, Finnish Meteorological Institute, Helsinki, Finland

Correspondence to: Frans Graeffe (frans.graeffe@helsinki.fi) and Mikael Ehn (mikael.ehn@helsinki.fi)

Abstract.

Alkanes are hydrocarbons that are emitted to the atmosphere mainly by human activities such as combustion processes and via the use of volatile chemical products (VCPs). They are an important group of volatile organic compounds (VOCs) that can produce secondary organic aerosol (SOA) in the atmosphere via hydroxyl (OH) radical initiated reactions. For many other compound groups (e.g., aromatics and monoterpenes), highly oxygenated organic molecules (HOMs) formed via autoxidation have been shown to be an important link between VOCs and SOA. Although alkane SOA has been intensively studied over the last decades, the importance of autoxidation and HOM in this system has received limited attention. The first HOM observations were only recently reported, but their relation so SOA has not been directly studied. Here, we show results of SOA yields from seven C$_{10}$ alkanes and their oxygenated derivatives in oxidation flow reactor experiments. We observe the well-known behaviour of increased SOA yield with different structure in the order of cyclic > linear > branched. We also measured HOMs, and all seven SOA precursors produced detectable amounts of products, but HOM quantification was not possible due to the experimental setup configuration focusing on SOA formation. However, a comparison to previously reported HOM yields for the same precursors was conducted, showing an overall correlation between HOM and SOA yields. Although not quantifiable, our own HOM observations did indicate that multi-generation OH oxidation played an important role in the SOA formation in our study.

1 Introduction

Alkanes are a major part of anthropogenic VOC (AVOC) emissions, especially in urban areas (Leuchner and Rappenglück, 2010; Garzón et al., 2015; Song et al., 2019; Gu et al., 2021). They mainly originate from combustion processes and vehicle exhaust (Jathar et al., 2017; Huang et al., 2018) as well as from volatile chemical products (VCPs), including adhesives, sanitiser, coatings and personal care products (Mcdonald et al., 2018; Wang et al., 2024). With the decrease of the traditional

anthropogenic VOC emissions, including the fossil fuel emissions from transportation/tailpipe emissions (Bishop and Haugen, 2018), other emissions can increase in relative importance, for example VCPs (Mcdonald et al., 2018; Coggon et al., 2021). As alkanes and their oxygenates are also part of VCPs, we need to understand better how they affect the air quality and SOA. The importance of VCP emissions have gotten more attention, and their significant contribution to urban emissions has only recently been addressed in more detail. Gu et al. (2021) found that alkanes (from e.g. mineral spirits) and aromatics were the major contributor to SOA-forming potential in Los Angeles county, USA, while Seltzer et al. (2021) found VCPs (including linear, cyclic and branched alkanes) a significant source of AVOC emissions in the USA. This demonstrates that more studies for these compounds are needed, as older measurements might not represent current AVOC emissions and compound specific distributions anymore.

Numerous previous studies have shown that alkanes are capable of producing significant amounts of SOA and the SOA yield depends among other things on the alkane carbon number and structure (Lambe et al., 2012; Tkacik et al., 2012; Hunter et al., 2014; Li et al., 2019; Hallward-Driemeier et al., 2024; Madhu et al., 2024; Jo et al., 2024).

Recently, Wang et al. (2021) showed that alkanes can undergo autoxidation more efficiently than previously thought, and have the potential to produce highly oxidized products, including those with more than six O-atoms, which are often labelled highly oxygenated organic molecules (HOM, (Bianchi et al., 2019)). Previous studies has shown that HOM production (via autoxidation) is an important link between VOCs and SOA for many systems, such as in the oxidation of monoterpene or aromatics (Ehn et al., 2014; Garmash et al., 2020). Wang et al. (2021) did not only measure HOM yields, but showed that the oxygen content in oxidation products generally increased with increasing bimolecular reaction rates, even though not always reaching six or more O-atoms. Much of the O-atom incorporation was attributed to reactions of peroxy radicals (RO_2) with other RO_2 radicals or NO, forming alkoxy radicals (RO) able to isomerize and thus allow reactions with molecular O_2. This is in contrast to many monoterpenes where the RO_2 radicals themselves can undergo isomerization reactions (autoxidation), owing to suitable structures in the monoterpene-derived radicals which are less common in alkanes.

In this study, we aim to extend the work of Wang et al. (2021) by measuring SOA yields for many of the alkanes and oxygenates that they reported, in order to assess the links between HOM and SOA formation. We produced atmospherically relevant SOA mass concentrations (<40 µg m^{-3}) from 7 different C_{10}-VOCs (alkanes and their oxygenated derivatives) to investigate their SOA yields. The experiments were done in an oxidation flow reactor, in the absence of NO_x and seed particles, simulating fresh SOA. We also measured HOMs at the exit of the flow reactor, but the experimental setup (optimized for SOA formation) did not allow direct quantification of the HOM yields.
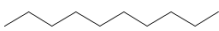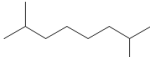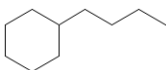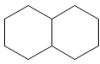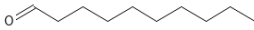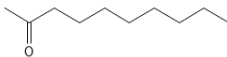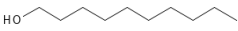
2 Methods

The experimental setup used in this work is presented in Fig. A1, and Table 1 summarises all the used VOCs. The instrumentation is described in the sections below.

65

Table 1. Summary of all the VOCs and their SOA yields.

Compound	Molecular formula	Structure	Injected VOC (ppb)	Reacted VOC (ppb)	Formed SOA-mass ($\mu g\ m^{-3}$)	SOA yield (%)
Alkane						
n-decane	$C_{10}H_{22}$		39-98	19-29	1.8-7.3	1.7-4.3
2,7-dimethyloctane	$C_{10}H_{22}$		29-12	16-32	0.59-7.6	0.65-4.6
n-butylcyclohexane	$C_{10}H_{20}$		14-110	10-33	9.4-38	13-25
cis-decalin	$C_{10}H_{18}$		16-79	12-30	14-76	21-44
Oxygenate						
decanal	$C_{10}H_{20}O$		13-52	11-28	1.4-27	2.0-16
2-decanone	$C_{10}H_{20}O$		43-120	21-33	1.2-17	0.89-8.3
1-decanol	$C_{10}H_{22}O$		120-360	33-41	6.4-23	2.9-8.8

2.1 SOA production with a PAM

70 We used a Potential Aerosol Mass oxidation flow reactor (PAM-OFR, hereafter PAM) (Kang et al., 2007; Lambe et al., 2011) to generate SOA via homogeneous nucleation from OH oxidation of the precursors. The PAM chamber is cylindrical and made of aluminium with a volume of ~13 L. Inside the PAM there are UV lamps, emitting at two wavelengths, 185 nm and 254 nm, producing oxidants according to: ozone (O_3) from oxygen (O_2), and hydroxyl radicals (OH) and hydroperoxyl radicals (HO_2) from water vapour (H_2O).

75 The total flow through the PAM was 10 L min^{-1}, consisting of purified air (clean air generator AADCO, series 737-14, Ohio, USA) that was directed through a water bath to increase the relative humidity (RH = 22 % ± 2 %) and a precursor gas flow

(N_2 as carrier gas). The residence time was therefore ~80 s. The VOC was continuously injected to the N_2 carrier gas flow with a syringe pump with different injection speeds to get different concentrations of the precursor to the PAM.

The flows, RH, and voltages of the UV lamps (100 V) were kept constant through all experiments, only the VOC concentration
80 was changing.

The integrated OH exposure was estimated by the estimation equation presented in Li et al. (2016), taking into account different SOA precursors and concentrations (with different reactivity toward OH and different external OH reactivity, OH_{ext}).

The integrated OH exposure (OH_{exp}) varied between 0.8×10^{10} and 8.6×10^{10} molecules cm^{-3} s in all of the experiments. Assuming atmospheric OH concentration of 1.5×10^6 molecules cm^{-3}, our experiments are equivalent to approximately 1 to 16
85 hours of atmospheric aging, i.e., fresh SOA.

Prior the actual measurements, we used a PTR-ToF (described in the section below) to measure OH_{exp} by measuring the decay of a compound at different UV intensities, as described in Lambe et al. (2011). Instead of using SO_2, the traditional choice, we used nonanal as it represents better the group of compounds used in this study. The measured OH_{exp} (at 35 ppb of nonanal) was 6.2×10^{10} molecules cm^{-3} s and the modelled OH_{exp} for the same calibration was 2.9×10^{10} molecules cm^{-3} s. A lower OH_{exp}
90 is expected for the model as it includes OH_{ext} while the measurement does not. However, as we used different precursors and measured over a wide range of precursor concentrations, and the discrepancy between the two methods were not huge, we chose to use the model to estimate OH_{exp}.

2.2 Instrumentation

Both particle and gas phase products were monitored after the PAM. Chemical composition of the freshly produced SOA was
95 measured with a Long Time of Flight Aerosol Mass Spectrometer (LToF-AMS, hereafter AMS) (Aerodyne Research, Inc.). (Decarlo et al., 2006; Graeffe et al., 2023) The AMS measured with 1 min acquisition. The sample flow to the AMS was 0.1 L min^{-1}, but we used an overflow of 1 L min^{-1} from the PAM to the AMS.

In order to bypass the problem of unknown/varying relative ionization efficiency (RIE) and collection efficiency (CE) for our pure organic aerosol in the AMS analysis, we used a custom-built scanning mobility particle sizer (SMPS) in conjunction with
100 the AMS for calculating the SOA mass concentration.

The AMS was used to calculate the elemental ratios (O/C and H/C) of the SOA, while the SMPS measured the particle number size distribution from 10 nm to 500 nm particles. From that, we also calculated the area and volume concentration.

The mass concentration of the SOA was calculated by combining the total particle volume from the SMPS and the SOA density calculated from the elemental ratios. The density was calculated for each step according to the equation in Kuwata et al. (2012),
105 yielding in densities from 1100 to 1400 kg m^{-3}.

For measuring HOMs, we used a nitrate chemical ionisation mass spectrometer (NO_3-CIMS) (Tofwerk AG/Aerodyne Research, Inc.) (Jokinen et al., 2012) equipped with a LToF and Eisele-type nitrate inlet (Eisele and Tanner, 1993). Our experimental setup was not optimized for the quantifying HOM yields, as our main goal was to study the SOA. The main

110 limitation for the HOM yield quantification was in determining the HOM loss rates. As the NO_3-CIMS needs a sample flow of ~10 L min^{-1} (i.e., sum of all the flows through the PAM), we needed to add a dilution flow directly after the PAM, making sure that all instruments got enough of sample flow. With this setup, we lost the majority of the HOMs coming from the PAM before they reached the NO_3-CIMS, owing to turbulence and related wall losses in the tubing. In addition, the vast majority of the HOMs produced in the PAM had already condensed onto particles or walls before exiting the PAM. Thus, a higher HOM

115 yield in the PAM may contribute to efficient SOA formation, which, in turn, forms a large sink for the HOM, ultimately decreasing the HOM concentrations. Due to these difficulties, we were not able to estimate the HOM losses and therefore not able to calculate any HOM yields. However, we were able to acquire mass spectra from all of the experiments and the HOM data collected did provide insights on the gas phase reactions.

For VOC measurements, we used a proton transfer reaction ToF mass spectrometer (PTR-ToF 8000, Ionicon Analytik GmbH,

120 Austria)(Jordan et al., 2009). However, the PTR-ToF was operational only during a few individual experiments, including the OH_{exp} calibration, so no detailed results from the actual experiments are shown here.

Ozone concentration was monitored with a photometric O_3 analyzer – model 400 (Teledyne API) and RH was kept constant during all experiments, RH = 22 % +- 2 %.

125 We injected typically 10-125 ppb of precursor VOC to the system, except for 1-decanol as it did not produce enough SOA at those precursor levels. For that, we injected up to 350 ppb to generate higher SOA loadings. The precursor was injected into a N_2 carrier gas with a syringe pump.

A typical experiment, showed in Fig. 1, consisted of the following steps: (1) background measurements with no VOC injected in the system, (2) different VOC concentrations injected to the system, producing $0 – 80$ µg m^{-3} of SOA and (3) background

130 measurements.
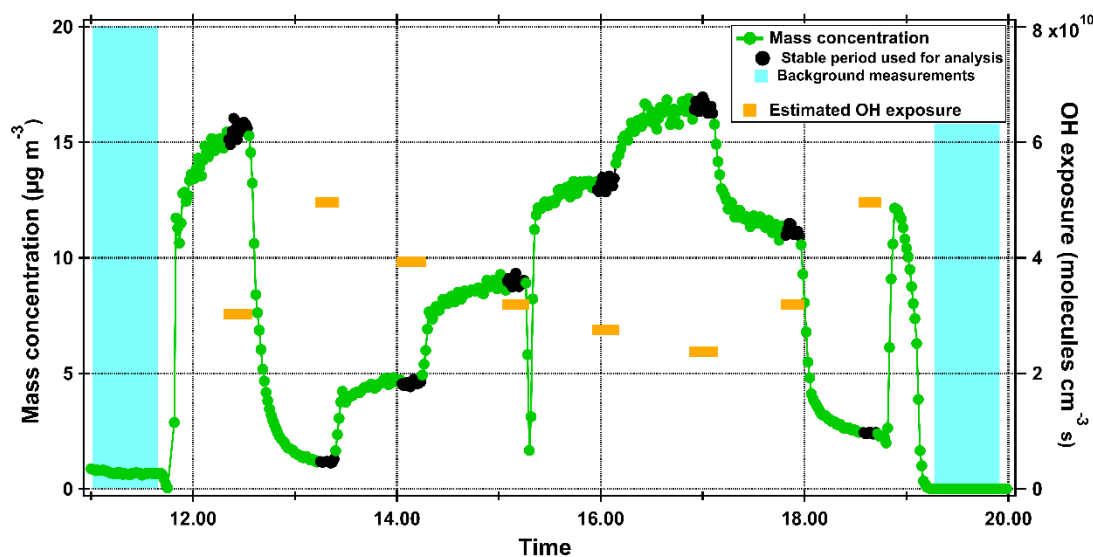
Figure 1. Time series of 2-decanone SOA mass concentration as an example of a typical experiment. The black points represent the stable time periods that were used for further analysis of a specific precursor/SOA mass concentration. The orange lines are the estimated OH exposures for each stable point and the blue region is the background period prior and after the precursor injections.

3 Results

3.1 Particle phase

3.1.1 SOA yields

The SOA yields (Y) are calculated as the ratio of formed organic aerosol concentration (C_{OA}) to reacted precursor concentration (ΔVOC) by:

$$Y = C_{OA}/\Delta VOC \tag{1}$$

The reacted precursor was calculated by:

$$\Delta VOC = [VOC] \times (1 - e^{-k \times OH_{exp}}) \tag{2}$$

, where k is the second-order rate constant of the precursor with OH and $[VOC]$ is the injected VOC concentration (known from the syringe pump).

The amount of reacted precursor varied from 10 to 41 ppb (Fig. 2b), corresponding to 25 % to 87 % of the injected amount of the precursor, expect for 1-decanol, which reacted only 11 % to 28 %.

In Fig. 2 we show the SOA yield as a function of injected VOC, reacted VOC and formed SOA. Summaries of the data from Figure 2 are also presented in Table 1. We can clearly see that the cycloalkanes and decanal had the highest SOA yields, ranging from ~2 % to ~44 %. The lowest SOA yields were from the acyclic alkanes and the other oxygenates (except decanal), ranging from ~0.07 % to ~9 %.

Our SOA mass concentrations were at atmospherically relevant levels (mostly below 20 µg m^{-3}) for all precursors. The compounds with high SOA yields, in particular the cycloalkanes, produced SOA efficiently already at low VOC concentrations, as seen in Fig. 2a and b. For example, cis-decalin produced on average over 19 µg m^{-3} of SOA at 10 ppb of reacted precursor, while 1-decanol did not produce any measurable mass below 30 ppb of reacted VOC. These results indicate

155 that the cycloalkane SOA is less volatile than the SOA from other precursors, as oxidation products are able to condense efficiently already at low concentrations. In contrast, the steep increases in SOA yields for many other precursors in Fig. 2b suggests that partitioning into the aerosol phase is strongly enhanced as the amount of products (and the SOA mass concentrations) increase.
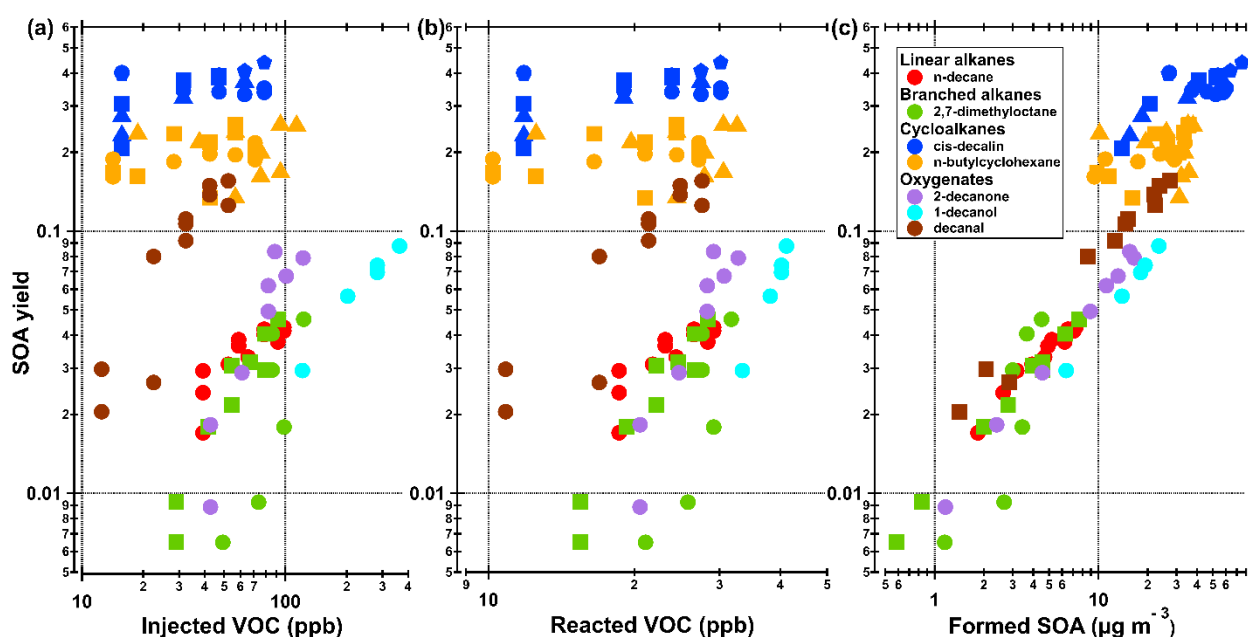
Figure 2. SOA yield as function of (a) injected VOC, (b) reacted VOC and (c) formed SOA. The different shapes of markers correspond to different experimental days of a specific precursor.

For alkanes, previous studies (Lim and Ziemann, 2005, 2009; Tkacik et al., 2012) have found that the SOA yield increases

165 following the trend cyclic > linear > branched. Although those studies were done in the presence of NO$_x$, while our study was done without any NO$_x$, we find the same overall behaviour for the SOA yields.

For n-decane, Presto et al. (2010) got a SOA yield of 1.5 % at 6 µg m^{-3} of SOA mass (under high NO$_x$ conditions), while we measured a yield of ~4 % at 6 µg m^{-3}. In the absence of NO$_x$, n-decane SOA yields have been studied also by Lambe et al.

170 (2012) and Li et al. (2019) in an OFR. However, both studies measured the SOA yields over different OH_{exp}, with emphasis

on more aged aerosol and the SOA yield evolution with increased OH_{exp}. Nevertheless, a SOA yield for n-decane from Lambe et al. (2012) and Li et al. (2019) would be less than 3 % at an equivalent photochemical age of ~0.5 days. Our SOA yields are therefore slightly higher with less ageing.

For cis-decalin, our SOA yield was 21-44 %, while Li et al. (2019) measured a SOA yield of 10 % at similar OH_{exp}.

175 For n-butylcyclohexane, the only reported SOA yield, 38 %, is from Lim and Ziemann (2009) where the experiment was done in presence of both seed aerosol and NO_x at over 1800 µg m^{-3} SOA mass concentrations. Therefore, their result is not directly comparable to our SOA yield of 13-25 %.

For the other precursors used in this study, we are not aware of any previous SOA yield measurements under similar conditions, i.e., in the absence of NO_x and seed aerosol.

180 **3.1.2 Van Krevelen diagram**
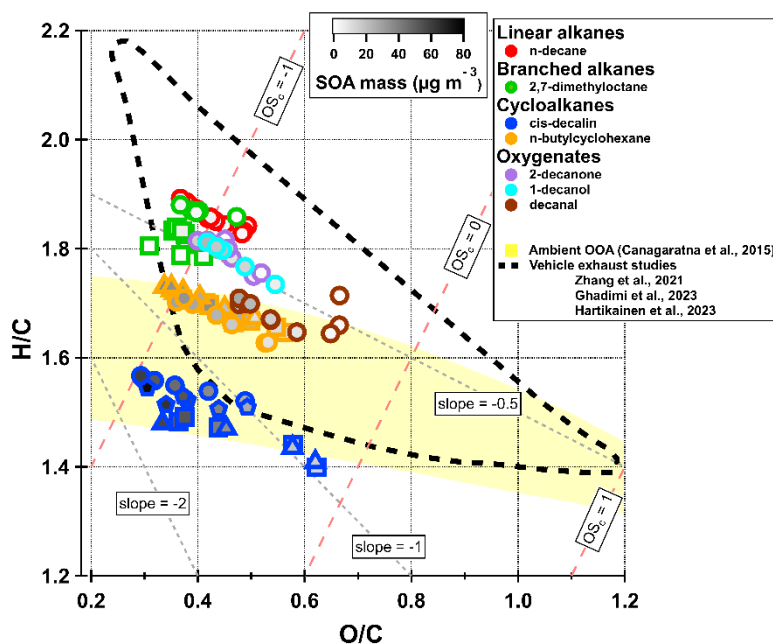
Figure 3. Van Krevelen diagram showing the H/C plotted against O/C. The different shapes of markers correspond to different
185 **experimental days of a specific precursor, while the inner color (white to black) corresponds to the SOA mass concentration of the data point. The red dashed lines correspond to estimated carbon oxidation states (OS_c) and the grey dashed lines are different slopes to guide the reader. The yellow shaded are represents the ambient H/C and O/C range of OOA according to Ng et al. (2011) and improved by Canagaratna et al. (2015). The area within the black dashed line represents data from recent vehicle emissions studies (Zhang et al., 2021; Ghadimi et al., 2023; Hartikainen et al., 2023).**

190 The oxygen to carbon (O/C) and hydrogen to carbon (H/C) ratios are plotted in a Van Krevelen diagram in Fig. 3. In general, for all compounds we clearly see that with increasing SOA mass concentration, the O/C ratio decreases and the H/C ratio

increases. This is in good agreement with previous studies (Shilling et al., 2009; Kuwata et al., 2012; Day et al., 2022). At low loadings, only the least volatile species, which are generally the most oxidized, are able to condense and form SOA, but as the particle mass increases, more volatile (and less oxidized) compounds can condense onto the particles, leading to decreased

195   O/C and increased H/C.

The H/C ratios of the SOA follows roughly the same order as the H/C ratios of the precursors (ranging from 1.8 to 2.2). Furthermore, our elemental ratios and slopes for cis-decalin and n-decane SOA are similar to those in Li et al. (2019).

The highest O/C ratios are observed for the high SOA-yield compounds (cis-decalin, butyl-cyclohexane and decanal) at low SOA mass concentration, indicating again that these compounds are efficient at producing low-volatility compounds that can

200   form SOA at low precursor concentrations.

Only the high-yield compounds go into the ambient H/C and O/C range (yellow area in Fig. 3, (Canagaratna et al., 2015)), while the other compounds have higher H/C ratio than the ambient range. The precursors in our study have quite high H/C ratio, which could explain why they are above the ambient H/C range. However, all data, except cis-decalin, falls into the area that represents recent vehicle exhaust studies (Zhang et al., 2021; Ghadimi et al., 2023; Hartikainen et al., 2023). As alkanes

205   are mostly anthropogenic emissions, these studies represent our experiment better than most typical ambient SOA studies, which can include biogenic SOA from precursors with typically much lower H/C ratios.

3.2 HOM comparison

210   We detected HOMs (compounds with six or more O-atoms) from all precursors and some example spectra are shown in Fig. A2-A8. While our own HOM measurements did not allow for yield determinations, we can compare the SOA yields from our study to the HOM yields from Wang et al. (2021). While the group of studied VOCs for our study was chosen from them, the experimental conditions are not the same. Wang et al. (2021) used a flow reactor with 3 s residence time and high VOC concentrations (~10 ppm), which also explains why they did not detect any second-generation oxidation while we did

215   (discussed in more detail below). However, a comparison is shown in Fig. 4, which shows our SOA yields versus the molar HOM yields in Fig. 3 from Wang et al. (2021). Figure 4 shows that decanal and cis-decalin had the highest HOM molar yields, which aligns well with our study as those two compounds belongs to the group of SOA yields compounds. Furthermore, they did not see any HOM signal for n-decane or 2,7-dimethyloctane (or measured it for 2-decanone), whereas we were able to get HOM signal from all of them. These 3 precursors also showed the lowest SOA yields. Although the comparison between our

220   study and Wang et al. (2021) is not ideal, this is the first comparison of HOM and SOA yields for alkanes and their oxygenates derivatives, and we can see a clear indication that higher HOM yields correlates with higher SOA yields.
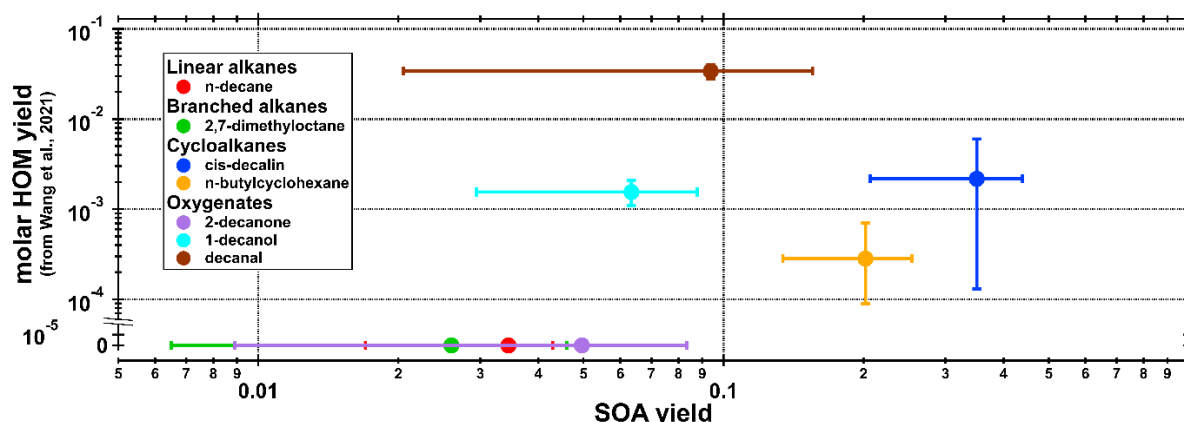
Figure 4. SOA yields (from Fig. 3) versus HOM yields (from Fig. 3 in Wang et al. (2021)). Datapoints are the average and the error
225 **bars represents the minimum and maximum of the measurements. For 2,7-dimethyloctane and n-decane, HOMs were not detected**
by Wang et al. (2021), and 2-decanone were not included in their HOM measurements. Therefore, the HOM yields for these three
compounds are assumed to be zero.

While our HOM data was not useful for quantification, the HOM distributions can be of use when assessing the role of multi-

generational OH oxidation. If we assume that the generic oxidation pathway for the precursors starts with H-abstraction by

230 OH, and potential radical propagation of peroxy or alkoxy radicals continue until radical termination takes place through the

loss of OH or HO_2, the formed products will have two H-atoms less than the precursors. If the products undergo another

reaction with OH, the second-generation oxidation products would have lost two additional H-atoms. As an example, in the

case of cis-decalin ($C_{10}H_{18}$), we would expect first-generation products to consist primarily of $C_{10}H_{16}O_z$ compounds under our

experimental conditions, while second-generation products would consist mainly of $C_{10}H_{14}O_z$ compounds. We indeed

235 observed a decreasing trend in the ratio of $C_{10}H_{14}O_y$ to $C_{10}H_{16}O_y$ (y=4-9) with increasing injected VOC concentration (Fig. 5),

indicating that lower precursor levels lead to increased second-generation OH oxidation in our system. This is to be expected,

as the OH generation stays largely constant, and thus high injected VOC concentrations will lead to the majority of OH radicals

reacting with the VOC. However, at lower injection rates, the VOC concentration will decrease significantly and there will be

more OH radicals available to react with oxidation products. Figure 5b shows the same ratios plotted versus the reacted amount

240 of VOC. The markers inner color (white to black), that shows the fraction of reacted VOC. At lower injection rates, a higher

fraction of the VOC is reacted, leaving more OH to react with oxidation products, while at higher injection rates, a lower

fraction (but a higher absolute concentration) is reacted. This expected behaviour can be seen for all precursors (Fig. 5). This

result, and the overall high values for these ratios (mostly around or above unity) suggest that multi-generation OH oxidation

is of importance in our experiments. For simplicity, as different compound ratios are calculated for the different precursors,

245 we will hereafter call the ratios $H_n:H_{n+2}$ ratio. Interestingly, the cyclic compounds, which also had the highest SOA yields,

show the highest value of the $H_n:H_{n+2}$ ratio. Speculating, if the cyclic compounds produce more oxidized products, which then

would have higher reactivity against OH, the number of second-generation products would be higher and therefore explain

this behaviour. The other compounds have lower values for the $H_n:H_{n+2}$ ratio, and go below unity at higher VOC concentrations.

This suggest that for 2,7-dimethyloctane, n-decane, 2-decanone and decanal second- (or multi-) generation oxidation is not as

250 important as for cis-decalin, n-butylcyclohexane and 1-decanol under these conditions.

255
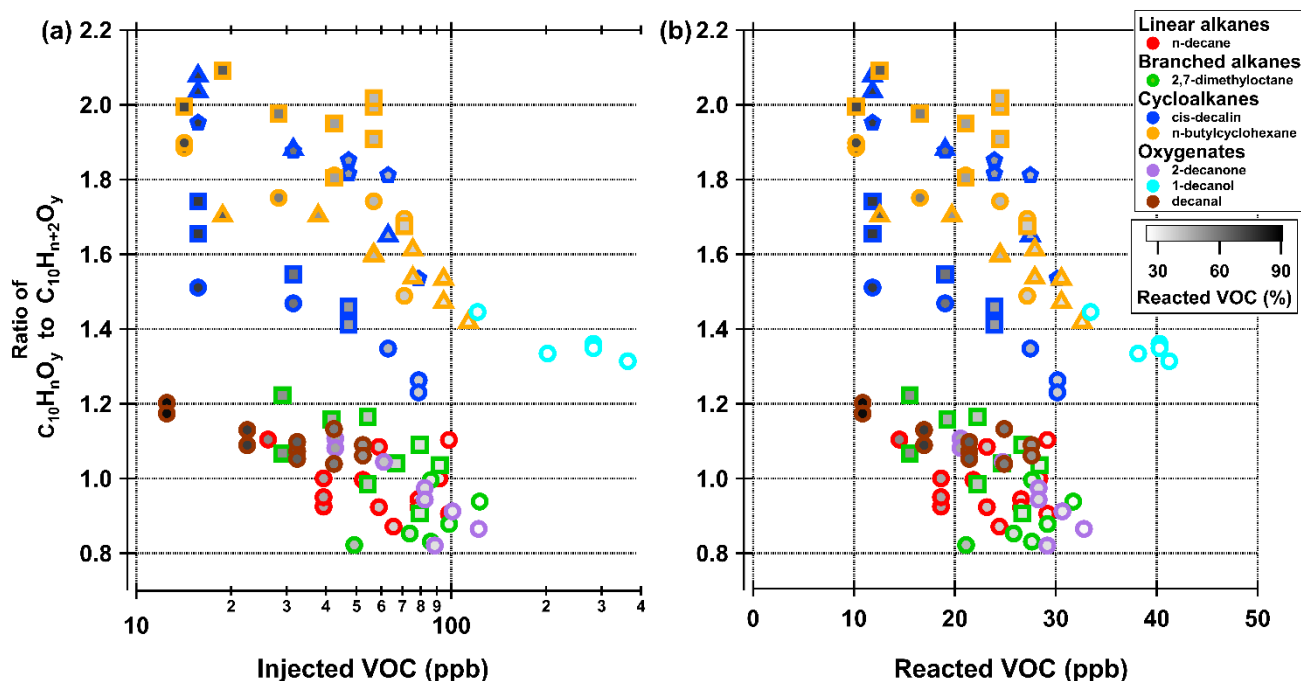
Figure 5. Ratios indicating the importance of multi-generation OH oxidation. The ratios on the y-axis are presented as $C_{10}H_nO_y/C_{10}H_{n+2}O_y$, with y=4-9 and n=14 for cis-decalin, n=16 for butyl-cyclohexane, 2-decanone and decanal, and n=18 for n-decane, 2,7-dimethyloctane and 1-decanol. The different shapes of markers correspond to different experimental days of a specific precursor, while the inner color (white to black) corresponds to the reacted VOC (%) of the data point. For visualization, the
260 **colorscale range is set from 25 % to 90 %, which includes all precursors except 1-decanol that ranges from 11 % to 28 %.**

4 Conclusions

We conducted experiments using a PAM chamber to measure SOA yields for seven C_{10} alkanes and their oxygenated

derivatives. The SOA formation was initiated by OH oxidation, in the absence of NO_x and seed aerosol. The conditions in the

265 PAM chamber were equivalent to approximately 1 to 16 hours of atmospheric aging, while producing atmospherically relevant

mass concentrations (<40 µg m^{-3}) of SOA. From our subset of C_{10} VOC, cis-decalin, decanal and n-butylcyclohexane showed

the highest SOA yields. For alkanes, the SOA yield increased in the order of cyclic > linear > branched alkanes, in accordance

with earlier observations. We also compared our SOA yields to previous reports of yields of highly oxygenated organic molecules (HOM)(Wang et al., 2021), finding that higher HOM yields indicates higher SOA yields.

270 In addition, we found clear differences in the contributions of multi-generational OH oxidation for the different precursors. This finding was based on assessing the amounts of H-atoms in the observed gas phase oxidation products that were measured from the PAM. In general, lower precursor concentrations enhanced multi-generational OH oxidation.

The primary aim of this study was to assess SOA yields of the C_{10} VOCs and compare them to observed HOM yields. Our findings suggest a clear link between the two yields, with compounds having low HOM yields also having low SOA yields.

275 However, the HOM and SOA yields were determined from different experiments under different conditions, meaning that quantification of the role of HOMs for the SOA formation is not possible from this work. In particular, the role of multigeneration OH oxidation was clearly higher in our study than in the one where HOM yields were determined, and even in our experiments there was considerable variation in the role of multigeneration oxidation between the VOCs. Overall, determining the exact chemical mechanism forming SOA from alkanes and their oxygenates will require further investigations,

280 but our findings clearly indicate that autoxidation and HOM formation should be accounted for when performing such investigations.

Appendix A: Supporting figures
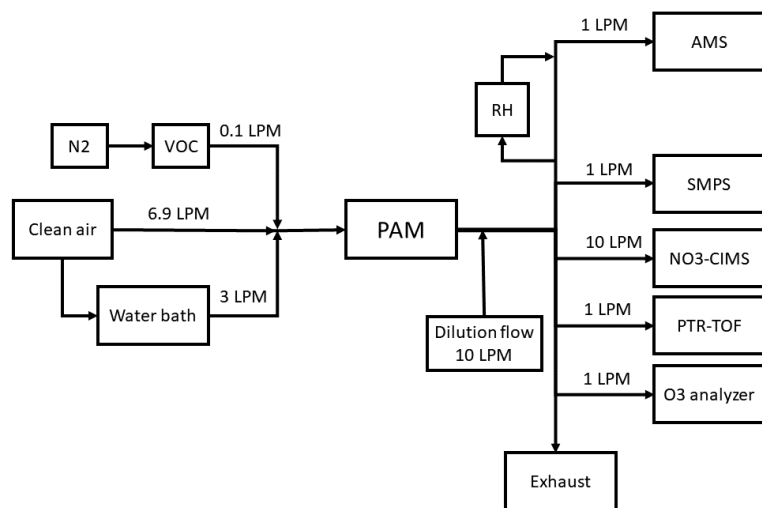
Figure A1. Experimental setup used in this work.

285
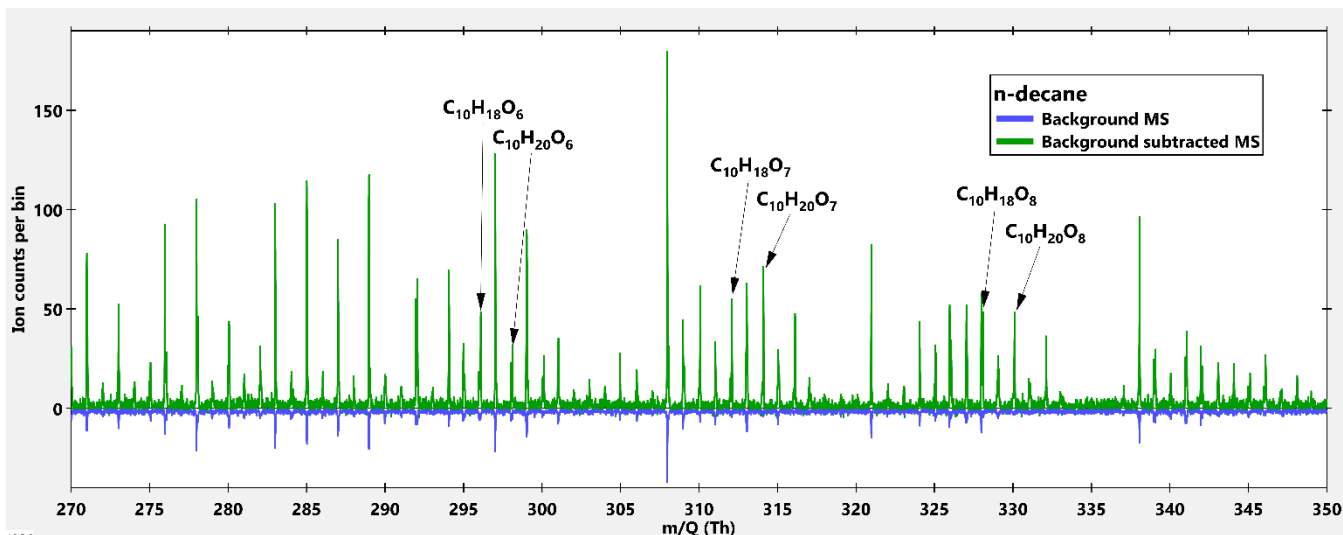
Figure A2. High resolution mass spectra (MS) of n-decane + OH. Blue MS is the background while the green MS is the background subtracted MS. The background MS is multiplied by a factor of -1 for visualization reasons.

290
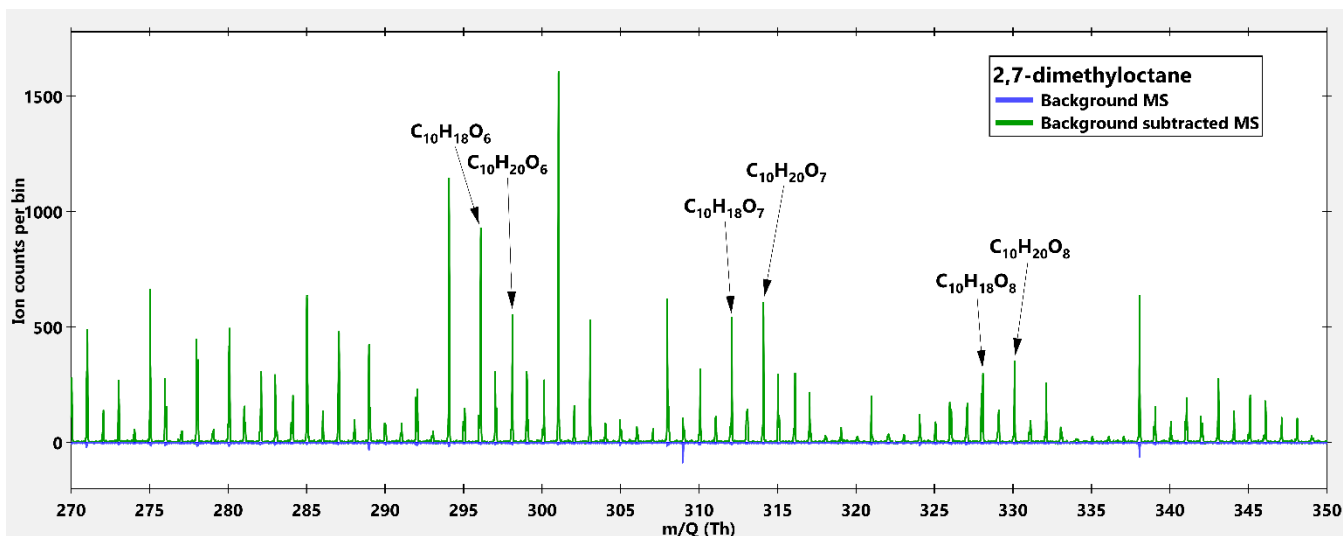
Figure A3. High resolution mass spectra (MS) of 2,7-dimethyloctane + OH. Blue MS is the background while the green MS is the background subtracted MS. The background MS is multiplied by a factor of -1 for visualization reasons.
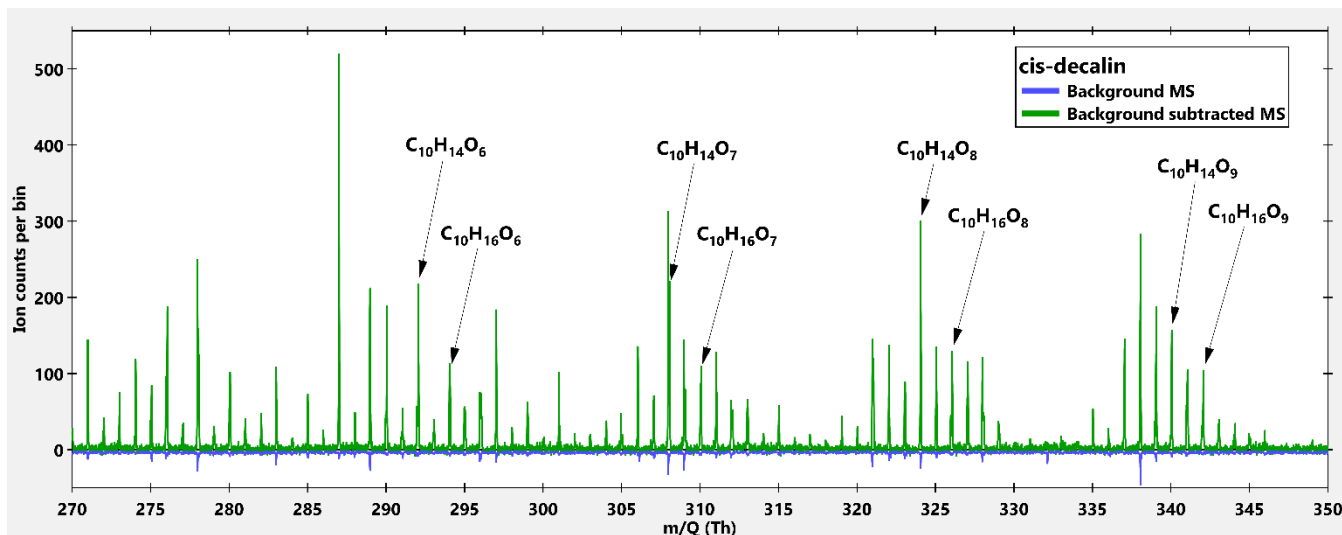
Figure A4. High resolution mass spectra (MS) of cis-decalin + OH. Blue MS is the background while the green MS is the background subtracted MS. The background MS is multiplied by a factor of -1 for visualization reasons.
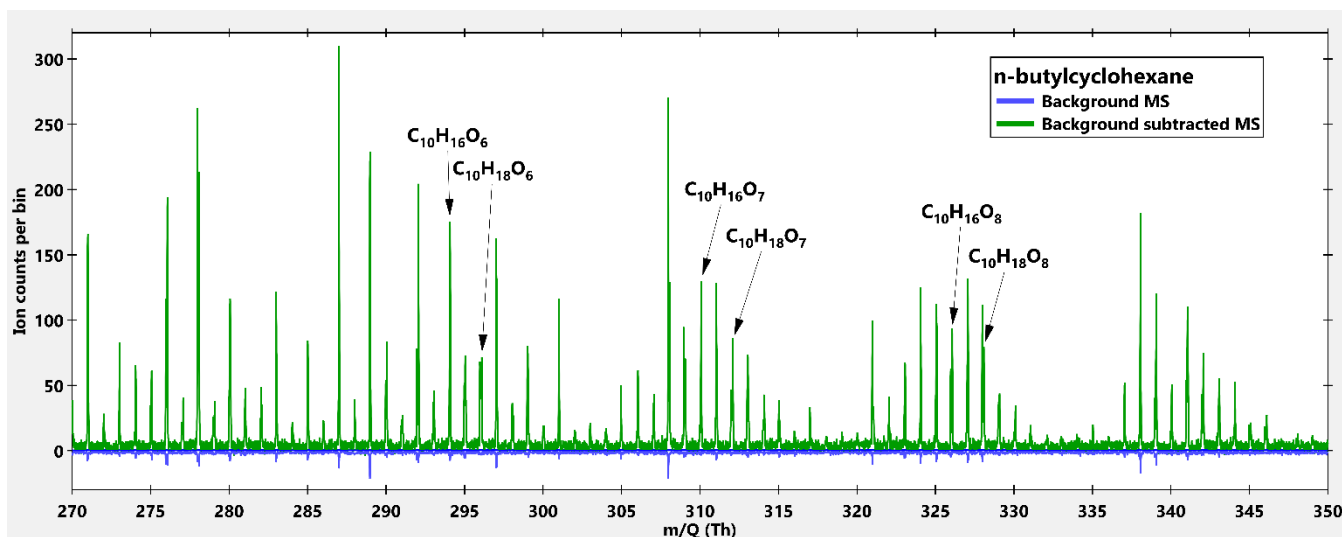
Figure A5. High resolution mass spectra (MS) of n-butylcyclohexane + OH. Blue MS is the background while the green MS is the background subtracted MS. The background MS is multiplied by a factor of -1 for visualization reasons.
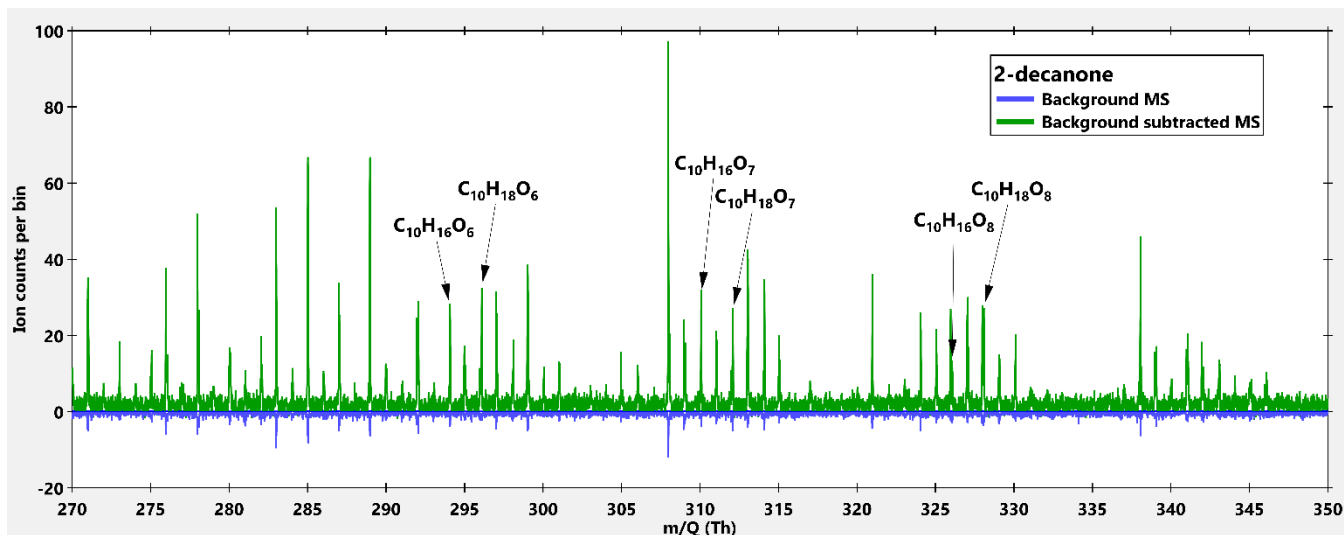
Figure A6. High resolution mass spectra (MS) of 2-decanone + OH. Blue MS is the background while the green MS is the background subtracted MS. The background MS is multiplied by a factor of -1 for visualization reasons.

305
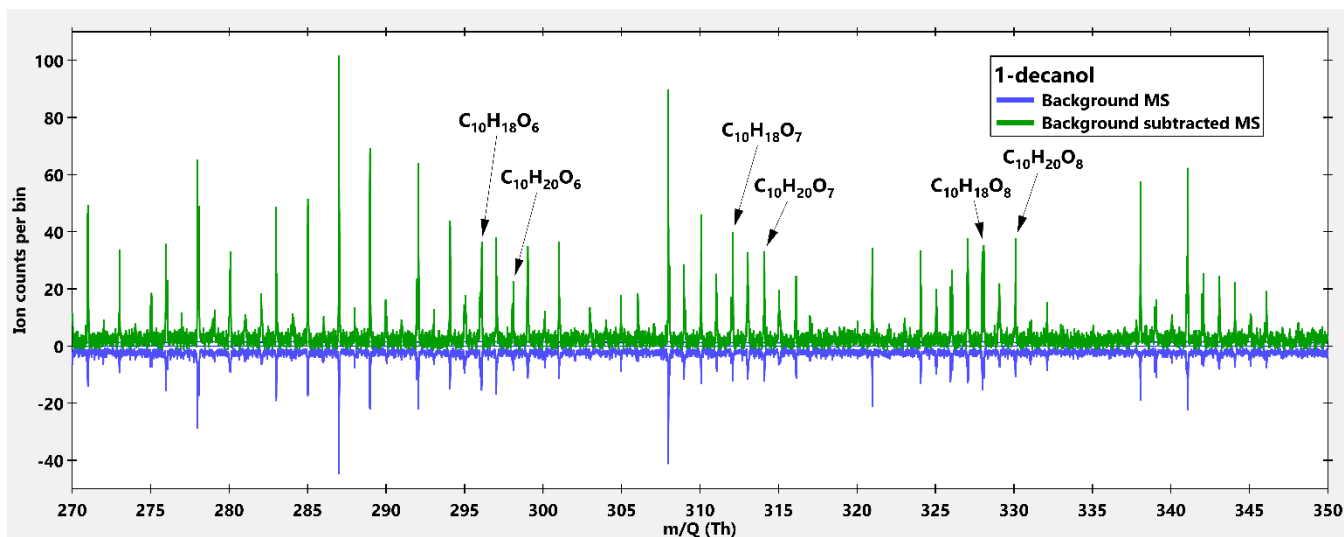
Figure A7. High resolution mass spectra (MS) of 1-decanol + OH. Blue MS is the background while the green MS is the background subtracted MS. The background MS is multiplied by a factor of -1 for visualization reasons.
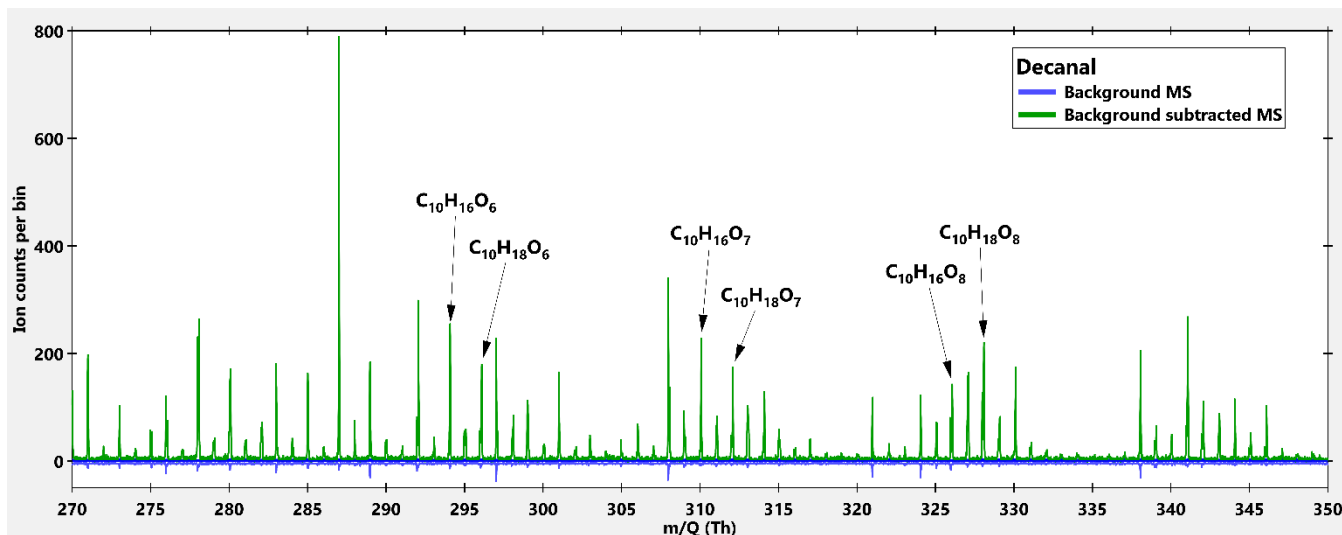
Figure A8. High resolution mass spectra (MS) of decanal + OH. Blue MS is the background while the green MS is the background subtracted MS. The background MS is multiplied by a factor of -1 for visualization reasons.

Data availability. Data are available upon request by contacting the corresponding author.

Author Contributions. ME designed the study. FG led the experiments with the help of KK. FG analysed the data. FG wrote the original draft. HT provided the PAM and support for its usage. All authors commented on the manuscript.

Competing interests. The authors declare that they have no conflict of interest.

Acknowledgments. This work was supported by the Academy of Finland (grants 320094, 317380 and 345982) and the Jane and Aatos Erkko foundation. Frans Graeffe thanks Svenska Kulturfonden for their support (grants 167344, 177923 and 188272).

References

Bianchi, F., Kurten, T., Riva, M., Mohr, C., Rissanen, M. P., Roldin, P., Berndt, T., Crounse, J. D., Wennberg, P. O., Mentel, T. F., Wildt, J., Junninen, H., Jokinen, T., Kulmala, M., Worsnop, D. R., Thornton, J. A., Donahue, N., Kjaergaard, H. G., and Ehn, M.: Highly Oxygenated Organic Molecules (HOM) from Gas-Phase Autoxidation Involving Peroxy Radicals: A Key Contributor to Atmospheric Aerosol, Chemical Reviews, 119, 3472-3509, 10.1021/acs.chemrev.8b00395, 2019.

Bishop, G. A. and Haugen, M. J.: The Story of Ever Diminishing Vehicle Tailpipe Emissions as Observed in the Chicago, Illinois Area, Environ. Sci. Technol., 52, 7587-7593, 10.1021/acs.est.8b00926, 2018.

Canagaratna, M. R., Jimenez, J. L., Kroll, J. H., Chen, Q., Kessler, S. H., Massoli, P., Hildebrandt Ruiz, L., Fortner, E., Williams, L. R., Wilson, K. R., Surratt, J. D., Donahue, N. M., Jayne, J. T., and Worsnop, D. R.: Elemental ratio measurements
335   of organic compounds using aerosol mass spectrometry: characterization, improved calibration, and implications, Atmos. Chem. Phys., 15, 253-272, 10.5194/acp-15-253-2015, 2015.
Coggon, M. M., Gkatzelis, G. I., McDonald, B. C., Gilman, J. B., Schwantes, R. H., Abuhassan, N., Aikin, K. C., Arend, M. F., Berkoff, T. A., Brown, S. S., Campos, T. L., Dickerson, R. R., Gronoff, G., Hurley, J. F., Isaacman-VanWertz, G., Koss, A. R., Li, M., McKeen, S. A., Moshary, F., Peischl, J., Pospisilova, V., Ren, X. R., Wilson, A., Wu, Y. H., Trainer, M., and
340   Warneke, C.: Volatile chemical product emissions enhance ozone and modulate urban chemistry, Proc. Natl. Acad. Sci. U. S. A., 118, 10.1073/pnas.2026653118, 2021.
Day, D. A., Fry, J. L., Kang, H. G., Krechmer, J. E., Ayres, B. R., Keehan, N. I., Thompson, S. L., Hu, W. W., Campuzano-Jost, P., Schroder, J. C., Stark, H., DeVault, M. P., Ziemann, P. J., Zarzana, K. J., Wild, R. J., Dubè, W. P., Brown, S. S., and Jimenez, J. L.: Secondary Organic Aerosol Mass Yields from NO3 Oxidation of α-Pinene and Δ-Carene: Effect of RO2 Radical
345   Fate, J. Phys. Chem. A, 126, 7309-7330, 10.1021/acs.jpca.2c04419, 2022.
DeCarlo, P. F., Kimmel, J. R., Trimborn, A., Northway, M. J., Jayne, J. T., Aiken, A. C., Gonin, M., Fuhrer, K., Horvath, T., Docherty, K. S., Worsnop, D. R., and Jimenez, J. L.: Field-deployable, high-resolution, time-of-flight aerosol mass spectrometer, Anal. Chem., 78, 8281-8289, 10.1021/ac061249n, 2006.
Ehn, M., Thornton, J. A., Kleist, E., Sipila, M., Junninen, H., Pullinen, I., Springer, M., Rubach, F., Tillmann, R., Lee, B.,
350   Lopez-Hilfiker, F., Andres, S., Acir, I. H., Rissanen, M., Jokinen, T., Schobesberger, S., Kangasluoma, J., Kontkanen, J., Nieminen, T., Kurten, T., Nielsen, L. B., Jorgensen, S., Kjaergaard, H. G., Canagaratna, M., Dal Maso, M., Berndt, T., Petaja, T., Wahner, A., Kerminen, V. M., Kulmala, M., Worsnop, D. R., Wildt, J., and Mentel, T. F.: A large source of low-volatility secondary organic aerosol, Nature, 506, 476-+, 10.1038/nature13032, 2014.
Eisele, F. L. and Tanner, D. J.: MEASUREMENT OF THE GAS-PHASE CONCENTRATION OF H2SO4 AND METHANE
355   SULFONIC-ACID AND ESTIMATES OF H2SO4 PRODUCTION AND LOSS IN THE ATMOSPHERE, J. Geophys. Res.: Atmos., 98, 9001-9010, 10.1029/93jd00031, 1993.
Garmash, O., Rissanen, M. P., Pullinen, I., Schmitt, S., Kausiala, O., Tillmann, R., Zhao, D. F., Percival, C., Bannan, T. J., Priestley, M., Hallquist, Å., Kleist, E., Kiendler-Scharr, A., Hallquist, M., Berndt, T., McFiggans, G., Wildt, J., Mentel, T., and Ehn, M.: Multi-generation OH oxidation as a source for highly oxygenated organic molecules from aromatics, Atmos.
360   Chem. Phys., 20, 515-537, 10.5194/acp-20-515-2020, 2020.
Garzón, J. P., Huertas, J. I., Magaña, M., Huertas, M. E., Cárdenas, B., Watanabe, T., Maeda, T., Wakamatsu, S., and Blanco, S.: Volatile organic compounds in the atmosphere of Mexico City, Atmos. Environ., 119, 415-429, 10.1016/j.atmosenv.2015.08.014, 2015.
Ghadimi, S., Zhu, H. W., Durbin, T. D., Cocker, D. R., III, and Karavalakis, G.: Exceedances of Secondary Aerosol Formation
365   from In-Use Natural Gas Heavy-Duty Vehicles Compared to Diesel Heavy-Duty Vehicles, Environ. Sci. Technol., 57, 19979-19989, 10.1021/acs.est.3c04880, 2023.
Graeffe, F., Heikkinen, L., Garmash, O., Äijälä, M., Allan, J., Feron, A., Cirtog, M., Petit, J. E., Bonnaire, N., Lambe, A., Favez, O., Albinet, A., Williams, L. R., and Ehn, M.: Detecting and Characterizing Particulate Organic Nitrates with an Aerodyne Long-ToF Aerosol Mass Spectrometer, Acs Earth and Space Chemistry, 7, 230-242,
370   10.1021/acsearthspacechem.2c00314, 2023.
Gu, S., Guenther, A., and Faiola, C.: Effects of Anthropogenic and Biogenic Volatile Organic Compounds on Los Angeles Air Quality, Environ. Sci. Technol., 55, 12191-12201, 10.1021/acs.est.1c01481, 2021.
Hallward-Driemeier, A. H., Hall, J. R., Spence, K. A., Telicki, B. P., Schaeffer, A. F., Avila, J. C., Albores, I. S., and Carrasquillo, A. J.: Secondary Organic Aerosol Formation and Chemistry from the OH-Initiated Oxidation of Monofunctional
375   C10 Species, Acs Earth and Space Chemistry, 8, 907-919, 10.1021/acsearthspacechem.3c00180, 2024.
Hartikainen, A. H., Ihalainen, M., Yli-Pirila, P., Hao, L. Q., Kortelainen, M., Pieber, S. M., and Sippula, O.: Photochemical transformation and secondary aerosol formation potential of Euro6 gasoline and diesel passenger car exhaust emissions, Journal of Aerosol Science, 171, 10.1016/j.jaerosci.2023.106159, 2023.
Huang, C., Hu, Q. Y., Li, Y. J., Tian, J. J., Ma, Y. G., Zhao, Y. L., Feng, J. L., An, J. Y., Qiao, L. P., Wang, H. L., Jing, S. A.,
380   Huang, D. D., Lou, S. R., Zhou, M., Zhu, S. H., Tao, S. K., and Li, L.: Intermediate Volatility Organic Compound Emissions from a Large Cargo Vessel Operated under Real-World Conditions, Environ. Sci. Technol., 52, 12934-12942, 10.1021/acs.est.8b04418, 2018.

Hunter, J. F., Carrasquillo, A. J., Daumit, K. E., and Kroll, J. H.: Secondary Organic Aerosol Formation from Acyclic, Monocyclic, and Polycyclic Alkanes, Environ. Sci. Technol., 48, 10227-10234, 10.1021/es502674s, 2014.

385 Jathar, S. H., Friedman, B., Galang, A. A., Link, M. F., Brophy, P., Volckens, J., Eluri, S., and Farmer, D. K.: Linking Load, Fuel, and Emission Controls to Photochemical Production of Secondary Organic Aerosol from a Diesel Engine, Environ. Sci. Technol., 51, 1377-1386, 10.1021/acs.est.6b04602, 2017.

Jo, Y., Jang, M., Han, S., Madhu, A., Koo, B., Jia, Y., Yu, Z., Kim, S., and Park, J.: CAMx-UNIPAR simulation of secondary organic aerosol mass formed from multiphase reactions of hydrocarbons under the Central Valley urban atmospheres of

390 California, Atmos. Chem. Phys., 24, 487-508, 10.5194/acp-24-487-2024, 2024.

Jokinen, T., Sipila, M., Junninen, H., Ehn, M., Lonn, G., Hakala, J., Petaja, T., Mauldin, R. L., Kulmala, M., and Worsnop, D. R.: Atmospheric sulphuric acid and neutral cluster measurements using CI-APi-TOF, Atmos. Chem. Phys., 12, 4117-4125, 10.5194/acp-12-4117-2012, 2012.

Jordan, A., Haidacher, S., Hanel, G., Hartungen, E., Märk, L., Seehauser, H., Schottkowsky, R., Sulzer, P., and Märk, T. D.:

395 A high resolution and high sensitivity proton-transfer-reaction time-of-flight mass spectrometer (PTR-TOF-MS), International Journal of Mass Spectrometry, 286, 122-128, 10.1016/j.ijms.2009.07.005, 2009.

Kang, E., Root, M. J., Toohey, D. W., and Brune, W. H.: Introducing the concept of Potential Aerosol Mass (PAM), Atmos. Chem. Phys., 7, 5727-5744, 10.5194/acp-7-5727-2007, 2007.

Kuwata, M., Zorn, S. R., and Martin, S. T.: Using Elemental Ratios to Predict the Density of Organic Material Composed of

400 Carbon, Hydrogen, and Oxygen, Environ. Sci. Technol., 46, 787-794, 10.1021/es202525q, 2012.

Lambe, A. T., Onasch, T. B., Croasdale, D. R., Wright, J. P., Martin, A. T., Franklin, J. P., Massoli, P., Kroll, J. H., Canagaratna, M. R., Brune, W. H., Worsnop, D. R., and Davidovits, P.: Transitions from Functionalization to Fragmentation Reactions of Laboratory Secondary Organic Aerosol (SOA) Generated from the OH Oxidation of Alkane Precursors, Environ. Sci. Technol., 46, 5430-5437, 10.1021/es300274t, 2012.

405 Lambe, A. T., Ahern, A. T., Williams, L. R., Slowik, J. G., Wong, J. P. S., Abbatt, J. P. D., Brune, W. H., Ng, N. L., Wright, J. P., Croasdale, D. R., Worsnop, D. R., Davidovits, P., and Onasch, T. B.: Characterization of aerosol photooxidation flow reactors: heterogeneous oxidation, secondary organic aerosol formation and cloud condensation nuclei activity measurements, Atmos. Meas. Tech., 4, 445-461, 10.5194/amt-4-445-2011, 2011.

Leuchner, M. and Rappenglück, B.: VOC source-receptor relationships in Houston during TexAQS-II, Atmos. Environ., 44,

410 4056-4067, 10.1016/j.atmosenv.2009.02.029, 2010.

Li, K., Liggio, J., Lee, P., Han, C., Liu, Q. F., and Li, S. M.: Secondary organic aerosol formation from α-pinene, alkanes, and oil-sands-related precursors in a new oxidation flow reactor, Atmos. Chem. Phys., 19, 9715-9731, 10.5194/acp-19-9715-2019, 2019.

Li, R., Palm, B. B., Ortega, A. M., Hlywiak, J., Hu, W. W., Peng, Z., Day, D. A., Knote, C., Brune, W. H., de Gouw, J. A.,

415 and Jimenez, J. L.: Modeling the Radical Chemistry in an Oxidation Flow Reactor: Radical Formation and Recycling, Sensitivities, and the OH Exposure Estimation Equation (vol 119, pg 4418, 2015), J. Phys. Chem. A, 120, 9886-9886, 10.1021/acs.jpca.6b11815, 2016.

Lim, Y. B. and Ziemann, P. J.: Products and mechanism of secondary organic aerosol formation from reactions of n-alkanes with OH radicals in the presence of NOx, Environ. Sci. Technol., 39, 9229-9236, 10.1021/es051447g, 2005.

420 Lim, Y. B. and Ziemann, P. J.: Effects of Molecular Structure on Aerosol Yields from OH Radical-Initiated Reactions of Linear, Branched, and Cyclic Alkanes in the Presence of NOx, Environ. Sci. Technol., 43, 2328-2334, 10.1021/es803389s, 2009.

Madhu, A., Jang, M., and Jo, Y.: Modeling the influence of carbon branching structure on secondary organic aerosol formation via multiphase reactions of alkanes, Atmos. Chem. Phys., 24, 5585-5602, 10.5194/acp-24-5585-2024, 2024.

425 McDonald, B. C., de Gouw, J. A., Gilman, J. B., Jathar, S. H., Akherati, A., Cappa, C. D., Jimenez, J. L., Lee-Taylor, J., Hayes, P. L., McKeen, S. A., Cui, Y. Y., Kim, S. W., Gentner, D. R., Isaacman-VanWertz, G., Goldstein, A. H., Harley, R. A., Frost, G. J., Roberts, J. M., Ryerson, T. B., and Trainer, M.: Volatile chemical products emerging as largest petrochemical source of urban organic emissions, Science, 359, 760-764, 10.1126/science.aaq0524, 2018.

Ng, N. L., Canagaratna, M. R., Jimenez, J. L., Chhabra, P. S., Seinfeld, J. H., and Worsnop, D. R.: Changes in organic aerosol

430 composition with aging inferred from aerosol mass spectra, Atmos. Chem. Phys., 11, 6465-6474, 10.5194/acp-11-6465-2011, 2011.

Presto, A. A., Miracolo, M. A., Donahue, N. M., and Robinson, A. L.: Secondary Organic Aerosol Formation from High-NOx Photo-Oxidation of Low Volatility Precursors: n-Alkanes, Environ. Sci. Technol., 44, 2029-2034, 10.1021/es903712r, 2010.

Seltzer, K. M., Pennington, E., Rao, V., Murphy, B. N., Strum, M., Isaacs, K. K., and Pye, H. O. T.: Reactive organic carbon
435   emissions from volatile chemical products, Atmos. Chem. Phys., 21, 5079-5100, 10.5194/acp-21-5079-2021, 2021.

Shilling, J. E., Chen, Q., King, S. M., Rosenoern, T., Kroll, J. H., Worsnop, D. R., DeCarlo, P. F., Aiken, A. C., Sueper, D., Jimenez, J. L., and Martin, S. T.: Loading-dependent elemental composition of α-pinene SOA particles, Atmos. Chem. Phys., 9, 771-782, 10.5194/acp-9-771-2009, 2009.

Song, C. B., Liu, B. S., Dai, Q. L., Li, H. R., and Mao, H. J.: Temperature dependence and source apportionment of volatile
440   organic compounds (VOCs) at an urban site on the north China plain, Atmos. Environ., 207, 167-181, 10.1016/j.atmosenv.2019.03.030, 2019.

Tkacik, D. S., Presto, A. A., Donahue, N. M., and Robinson, A. L.: Secondary Organic Aerosol Formation from Intermediate-Volatility Organic Compounds: Cyclic, Linear, and Branched Alkanes, Environ. Sci. Technol., 46, 8773-8781, 10.1021/es301112c, 2012.

445   Wang, S. H., Yuan, B., He, X. J., Cui, R., Song, X., Chen, Y. B., Wu, C. H., Wang, C. M., Huangfu, Y. B., Li, X. B., Wang, B. G., and Shao, M.: Emission characteristics of reactive organic gases (ROGs) from industrial volatile chemical products (VCPs) in the Pearl River Delta (PRD), China, Atmos. Chem. Phys., 24, 7101-7121, 10.5194/acp-24-7101-2024, 2024.

Wang, Z. D., Ehn, M., Rissanen, M. P., Garmash, O., Quéléver, L., Xing, L. L., Monge-Palacios, M., Rantala, P., Donahue, N. M., Berndt, T., and Sarathy, S. M.: Efficient alkane oxidation under combustion engine and atmospheric conditions,
450   Communications Chemistry, 4, 10.1038/s42004-020-00445-3, 2021.

Zhang, Z. R., Zhu, W. F., Hu, M., Liu, K. F., Wang, H., Tang, R. Z., Shen, R. Z., Yu, Y., Tan, R., Song, K., Li, Y. J., Zhang, W. B., Zhang, Z., Xu, H. M., Shuai, S. J., Li, S. D., Chen, Y. F., Li, J. Y., Wang, Y. S., and Guo, S.: Formation and evolution of secondary organic aerosols derived from urban-lifestyle sources: vehicle exhaust and cooking emissions, Atmos. Chem. Phys., 21, 15221-15237, 10.5194/acp-21-15221-2021, 2021.

455